Tailoring adsorption induced phase transitions in the pillared-layer type metal-organic framework DUT-8(Ni)

Kavoosi, Negar; Bon, Volodymyr; Senkovska, Irena; Krause, Simon; Atzori, Cesare; Bonino, Francesca; Pallmann, Julia; Paasch, Silvia; Brunner, Eike; Kaskel, Stefan. Tailoring adsorption induced phase transitions in the pillared-layer type metal-organic framework DUT-8(Ni). DALTON TRANSACTIONS. 46 (14) pp: 4685-4695.
DOI: 10.1039/C7DT00015D

Tailoring adsorption induced phase transitions in the pillared-layer type metal-organic framework DUT-8(Ni)

Negar Kavoosi,[a] Volodymyr Bon,[a] Irena Senkovska,[a] Simon Krause,[a] Cesare Atzori,[b] Francesca Bonino,[b] Julia Pallmann,[c] Silvia Paasch,[c] Eike Brunner[c] and Stefan Kaskel[a*]

Tailoring the characteristics of gating transitions in the porous network, $Ni_2(ndc)_2dabco$ (ndc = 2,6-naphthalenedicarboxylate, dabco = 1,4-diazabicyclo[2.2.2]octane), also termed DUT-8(Ni) (DUT = Dresden University of Technology), was achieved by systematically adjusting the critical synthesis parameters. The impact of the starting composition and solvent mixtures in the synthesis was found to critically affect the guest-response properties of the obtained materials. A comprehensive set of physical characterization methods, namely thermal analysis, ^{1}H NMR of digested crystals, solid state ^{13}C NMR, PXRD, SEM, IR and Raman spectroscopy shows that the crystallite size is a crucial factor, determining the differing characteristics such as "gate pressure" and adsorption capacity in the guest-responsive switching behaviour of DUT-8. Crystallites smaller than 500 nm in size retain the open form after removal of the guest molecules resulting in typical "Type I" isotherms, whereas crystallites larger than 1 µm transform into the "closed pore" form and therefore can show a characteristic "gate opening" behaviour during the gas adsorption. The particle size distribution of DUT-8(Ni) can be tailored by changing the synthesis conditions and consequently the slope of the isotherm at the "gating step" is affected. The in depth analysis of synthesis conditions and switching behaviour is an important step towards a better understanding of the fundamental principles responsible for guest responsive porosity switching in the solid state.

Introduction

Structural phase transitions induced by external stimuli such as guest molecules, temperature, electromagnetic irradiation etc., are unique features of flexible metal-organic frameworks, also termed soft porous crystals.[1-4] Among various kinds of flexibility such as breathing, swelling, ligand flip, sub-network displacement, *gating* stands out as a pronounced and step-wise transition with an amplitude of cell volume change often by far exceeding any volume changes observed in traditional porous solids.[5] We therefore address these materials in the following as "switching MOFs" or "gate pressure MOFs". After guest removal, "gate pressure MOFs" usually transform into a dense structure that can be reopened by an external stimulus.[6] Switching between a "porous" and "non-porous" (or dense) state offers tremendous opportunities for the application of these MOFs in gas storage, separation, and sensing.[7-16] However, there are still numerous open questions in the understanding of "gating" phenomena from both experimental and theoretical point of view.

From the theoretical point of view, various fundamental concepts for understanding the flexible behaviour were developed, for example: (i) the adsorption-induced deformation can be interpreted as a response of the porous material to an adsorption induced stress; (ii) a rigorous thermodynamic description of the coupled energetics of the crystallographic phase transition(s) and the adsorption isotherms of the different polymorphs within the osmotic ensemble.[17, 18]

The synthesis rules and procedures for the targeted synthesis of "gate pressure" materials and control over the "gate pressure" is a crucial issue for any application. In the case of layered MOFs such as ELM-11 (ELM – Elastic Layered Material), the first "gate pressure MOF" discovered, extensive investigations focussed on the adsorption induced transitions in the presence of nitrogen, carbon dioxide, *n*-butane, methane, and alcohol vapours.[6, 19-21] Tuning of the "gate pressure" was achieved by varying the metal ions and type of layer-terminating anions.[22] The dynamics of the "gating" effect was investigated *in situ* using various gases as guest molecules.[23]

Pillared-layer MOFs can be regarded as a second prototypical class of switching MOFs as discovered by Dybtsev,[24] but initially only volume changes below 15% were reported in the absence of solvent. However, a complete closing of the framework was not achieved in this case.

A unique member of this family is $Ni_2(ndc)_2dabco$ (ndc – 2,6-naphtalenedicarboxylate, dabco - 1,4-diazabicyclo-[2.2.2]octane), also known as DUT-8(Ni) (DUT = Dresden University of Technology).[25-30] The highly flexible Ni_2-paddle wheel in combination with the ndc ligand allows to achieve the complete pore closing after removing the guest molecules. Consequently this compound shows the highest cell volume change (> 250 %) among all pillared layer MOFs and a pronounced "gate opening" effect, initially reported at $p/p_0 = 0.1$ for nitrogen adsorption at 77 K.[29] The complex structural diversity of DUT-8(Ni) in the presence of nitrogen, carbon dioxide, ethane, ethylene3 and *n*-butane was unravelled using *in situ* powder X-ray diffraction (PXRD) at controlled pressure and temperature.[26] Characteristic host-guest interactions were detected applying *in situ* ^{129}Xe NMR.[31]

However, recent observations during repeated adsorption/desorption cycling using *n*-butane and InfraSORP technology revealed significant stress built-up upon repeated adsorption caused by grain boundary formation and disintegration of larger crystals.[27] Three different type of crystal interfacial surface areas may in principal affect the gating phenomena by adding a kinetic and/or thermodynamic contribution to alter the energetics of switching: a) the outer surface area (A_o) of a monodomain crystal (surface energy); b) the interfacial area between two domains (grain boundary or interfacial domain area, A_{id}) with different orientation in one crystal; c) the interfacial area of a monodomain or multidomain crystal covered by a second phase (which can be also an amorphous outer layer (A_{ol}), a polymer, or a crystalline shell). For DUT-8, it was shown that an increasing A_{id} causes a shift of the gate opening pressure to higher pressure (equivalent to higher chemical potential of the guest molecule)[27]. As we show in this contribution, the gate opening pressure does not reflect a transition at equilibrium, but is kinetically controlled. The concerted pore opening of unit cells can be interpreted as a cooperative lattice movement (soft phonon) propagating throughout the crystal. If adjacent grains have different crystallographic orientation, the interfacial domain area (grain boundary) acts as a phonon propagation barrier and shifts the transition pressure towards higher chemical potential of the transition inducing guest molecules. However, if the interface between two domains

creates gas accessible channels, these defects will act as nucleation centers for the phase transformation. Thus, the number of such defects in a crystal will determine the transition probability and consequently the gate opening pressure. A monodomain crystal without grain boundaries in the closed state may be kinetically so severely hindered, that an adsorption induced transition is not any longer observed and the crystal remains closed.

The strong influence of domain size on "gate pressure" was an initial motivation to study the impact of crystal morphology in DUT-8(Ni) in more detail. Another observation triggering our intentions for "gate pressure" tuning came from a report by Lee et al. who reported the material with the same structure and composition as for DUT-8(Ni) but described it as a rigid MOF with a clear "Type I" isotherm and no structural transformations during the guest removal.[32] This material was synthesized using slightly modified synthesis conditions.

Consequently, DUT-8(Ni) is a unique solid, showing either switchable or rigid behaviour depending on the way it is synthesized. So far there are only few reports describing a synthesis dependent switchability tuning in porous solids.[9, 33, 34, 35]

In the following we describe a detailed study on synthesis and pre-treatment parameters affecting "gate pressure" and hysteresis in DUT-8(Ni). In order to elucidate the fundamentals of solid state porosity switching and in the context of the textural characteristics behind, we have focussed on a global analysis using various spectroscopic techniques, scanning electron microscopy, elemental analysis, TG etc. and correlated the outcome with gas physisorption results revealing the degree of switchability.

Experimental

Materials

Chemicals and solvents were purchased from Sigma Aldrich and they were used without further purification. Nickel (II) nitrate hexahydrate (99.999%), 2,6-naphthalenedicarboxylic acid (99.0%) and 1,4-diazabicyclo[2.2.2]octane (ReagentPlus®, ≥99%) were handled under inert atmosphere. *N,N*-Dimethylformamide (99.8%) and methanol (99.8%) were purchased in anhydrous form.

Synthesis

Flexible DUT-8(Ni) (1)

The synthesis procedure of DUT-8(Ni) reported in ref. [29] was slightly modified insofar as all chemicals were dissolved separately: $Ni(NO_3)_2{\cdot}6H_2O$ (0.407 g, 1.40 mmol) in 6 mL DMF, H_2ndc (0.303 g, 1.40 mmol) in 15 mL DMF and dabco (0.100 g, 0.89 mmol) in 9 mL methanol (MeOH). Subsequently the mixture was transferred into a Teflon vessel (50 mL) and heated in an autoclave to 393 K with a heating rate of 4 K/min and held at that temperature for 48 h. After cooling to room temperature (RT) during 3 hours, the sample was washed several times, first with 30 mL DMF and then with 30 mL ethanol and at the end with 30 mL DCM. Afterwards, the washing step with 150 mL of DCM was continued for 3 days. The resulting solid was filtered in argon flow and activated in dynamic vacuum at 393 K for 4 h. DUT-8(Ni) crystals have poor heat conductivity, therefore for efficient activation of sample it is important to prevent aggregation of the crystals. In order to facilitate the homogeneous heat transfer to all crystallites instantly without solvothermal stress during the desolvation, a flask with a wide flat bottom was used. This method allows for a homogeneous heating of all the crystals without temperature gradients and simultaneous evacuation. Note: A special vacuum safe flask is required for this operation. Evacuation (at 10^{-3} mbar) continued over night at room temperature. During the activation, the colour of the sample changes from green (open pore phase) to dark yellow (closed pore phase). Finally, the Schlenk tube was purged with argon and transferred into the Glove Box.

Rigid DUT-8(Ni) (2)

The "rigid" form of DUT-8(Ni) was synthesized using a similar procedure as reported by Lee et al.[32] In a typical synthesis, $Ni(NO_3)_2{\cdot}6H_2O$ (0.434 g, 1.50 mmol), H_2ndc (0.294 g, 1.36 mmol) and dabco (0.336 g, 3.00 mmol) were mixed and dissolved in 30 mL of DMF using an ultrasonic bath for 10 min. After mixing of all chemicals, a cloudy suspension was obtained, which is in disagreement with the procedurereported by Lee. A clear solution could not be obtained even after ultrasonication of the cloudy precipitate for 2 hours. The suspension was placed in a Teflon-lined autoclave and heated in an oven to 408 K with a heating rate of 4 K/min and held at that temperature for 72 hours. The resulting material was washed with 30 mL DMF two times and subsequently immersed in 30 mL of dry EtOH for 3 days. The light green powder was filtered out and activated in dynamic vacuum for 5 hours at 443 K. After activation, the colour remained light green. The sample was kept under inert atmosphere.

Variation of dabco content: series 3

Samples **a-d** of series **3** were synthesized using the same procedure as described for **2**, but utilising varying amounts of dabco. In all the cases, the ratio of Ni^{2+}:H_2ndc 1.1:1 was kept constant (0.434 g Ni^{2+}, 0.294 g H_2ndc). The following amounts of dabco were utilised: in $\mathbf{3_a}$ 0.030 g (0.27 mmol), in $\mathbf{3_b}$ 0.058 g (0.52 mmol), in $\mathbf{3_c}$ 0.112 g (1.00 mmol) and in $\mathbf{3_d}$ 0.224 g (2.00 mmol).

Variation of dabco content: series 3'

Samples **a-d** of series **3´** were synthesized using the procedure described for **1**. For all the samples, a constant ratio of Ni^{2+}:H_2ndc 1:1 was used (0.407 g Ni^{2+}, 0.303 g H_2ndc). The amount of dabco was varied as follows: in $\mathbf{3´_a}$ 0.039 g (0.35 mmol), in $\mathbf{3´_b}$ 0.100 g (0.89 mmol), in $\mathbf{3´_c}$ 0.156 g (1.39 mmol) and in $\mathbf{3´_d}$ 0.336 g (3.00 mmol).

Variation of solvents ratio: series 4

All samples were synthesized using procedure described for **2,** but the ratio of solvents (DMF to MeOH) was varied: in **4_a** 29.5 mL DMF and 0.5 mL MeOH, in **4_b** 25 mL DMF and 5 mL MeOH, and in **4_c** 19 mL DMF and 11 mL MeOH.

Variation of nickel to ligands ratio: series 5

Samples **a-b** of series **5** were synthesized with the same method used for preparation of sample **2**, but the ratio of Ni to other compounds was changed. In both cases, a ratio of H_2ndc:dabco = 1:2.2 was used (0.294 g H_2ndc, 0.336 g dabco). In the case of **5_a**, 0.394 g (1.35 mmol) of $Ni(NO_3)_2{\cdot}6H_2O$ and in **5_b**, 0.197 g (0.68 mmol) of $Ni(NO_3)_2{\cdot}6H_2O$ was added.

Variation of nickel content: series 5´

Samples **a** and **b** of series **5´** were synthesized using the same procedure as described for **1** but the ratio of Ni to other components was changed. In **5´$_a$** 0.204 g (0.70 mmol) $Ni(NO_3)_2{\cdot}6H_2O$ and in **5´$_b$** 0.601 g (2.07 mmol) $Ni(NO_3)_2{\cdot}6H_2O$ were used and in both cases, the ratio of H_2ndc to dabco was kept constant (0.303 g H_2ndc, 0.1 g dabco).

Table1. Synthesis parameters used for tuning DUT-8(Ni) materials[1]

	Ni^{2+}	H_2ndc	dabco	MeOH mL	DMF mL	T, K / sonication time, min
1	1.0	1.0	0.636	9.0	21.0	393/10
2	1.1	1.0	2.206	-	30.0	408/10
3_a	1.1	1.0	0.199	-	30.0	408/10
3_b	1.1	1.0	0.382	-	30.0	408/10
3_c	1.1	1.0	0.735	-	30.0	408/10
3_d	1.1	1.0	1.470	-	30.0	408/10
3'$_a$	1.0	1.0	0.250	9.0	21.0	393/10
3'$_b$	1.0	1.0	0.636	9.0	21.0	393/10
3'$_c$	1.0	1.0	0.993	9.0	21.0	393/10
3'$_d$	1.0	1.0	2.143	9.0	21.0	393/10
4_a	1.1	1.0	2.206	0.5	29.5	408/10
4_b	1.1	1.0	2.206	5.0	25.0	408/10
4_c	1.1	1.0	2.206	11.0	19.0	408/10
5_a	1.0	1.0	2.206	-	30.0	408/10
5_b	0.5	1.0	2.206	0.0	30.0	408/10
5'$_a$	0.5	1.0	0.636	9.0	21.0	393/10
5'$_b$	1.5	1.0	0.636	9.0	21.0	393/10

[1]For the starting compounds, the molar ratio normalized to H_2ndc is given.

Powder X-ray diffraction

Powder X-ray diffraction (PXRD) patterns were measured at room temperature on a STOE STADI P diffractometer using Cu–$K_{\alpha1}$ radiation (λ = 1.5405 Å) and a 2D detector (Mythen, Dectris). All measurements were performed in transmission geometry using a rotating flatbed sample holder, 2Θ steps of 0.015° and exposition time of 20 s per step. All activated samples were sealed using decathlon aptonia survival blanket (film composition: 4.0% Resin, 92.0% polytetrafluoroethylene (PTFE), 4.0% aluminium).

Adsorption

Nitrogen (at 77 K) and argon (at 87 K) physisorption experiments were performed using a BELSORP-max apparatus. A liquid nitrogen bath was used to thermostat the sample at 77 K. Argon physisorption measurements were performed using a special external adsorption cell, mounted on a closed cycle He-cryostat. Measurements were carried out using 25 - 35 mg of the MOF. For all experiments, nitrogen and argon gases with purity of 99.999% were used.

Thermogravimetric analyses

Thermogravimetric analyses (TG) were performed in synthetic air flow in a temperature range from room temperature to 1000 °C with a heating rate of 5 °C/min using STA 409 PC from NETZSCH Company.

Spectroscopic measurements

DRIFT spectra were measured in the range of 4000 - 400 cm^{-1} using a VERTEX-70 spectrophotometer (Bruker).

FTIR ATR spectra were collected at 2 cm^{-1} resolution in the 4000 - 400 cm^{-1} range using a Bruker Alpha instrument equipped with an ATR

accessory (diamond crystal) and placed inside the Glove Box. Raman spectra were recorded on powder samples inserted in a home-made cell with a suprasil quartz cuvette by using a Renishaw inVia Raman microscope spectrometer and an Ar^+ laser emitting at 514 nm. Photons scattered by the sample were dispersed by a 1800 lines/mm grating monochromator and were simultaneously collected on a CCD camera. The collection optic was set at 20X. The spectral collection setup consisted of 50 acquisitions, each of 10 s.

Scanning electron microscopy

The SEM images were recorded using a Hitachi Microscope SU8020.

Elemental analysis

The CHN analysis was performed on a EuroEA Elemental Analyser. The amount of Ni in the samples was determined by ICP-OES using an Optima 7000 DV instrument.

Nuclear magnetic resonance

The solutions for ^{1}H NMR were prepared by dissolving the activated samples in a mixture of 1 mL (99.9%) dimethyl sulfoxide-d_6 and 20 µl of DCl (36% solution in D_2O). The spectra were measured on a Bruker DRX-500 spectrometer. Solid-state ^{13}C NMR experiments were performed on a Bruker AVANCE 300 spectrometer operating at a resonance frequency of 75.5 MHz using a double-resonance 4 mm MAS NMR probe and a sample spinning rate of 12 kHz. Ramped ^{1}H-^{13}C cross polarization (CP) and SPINAL proton decoupling during signal acquisition was applied. The chemical shift was referenced with adamantane.

Results and Discussion

To identify pivotal parameters responsible for the differences in the switching characteristics of $Ni_2(ndc)_2(dabco)$ it was essential to reproduce the syntheses of “flexible” and “rigid” materials, in the following denoted as **1** and **2**, respectively. For the synthesis of **1** the amount of dabco was slightly increased[29] to improve the yield. When following the reported procedure for the synthesis of “rigid” DUT-8(Ni) (**2**) reported by Lee et al.[32] the solution became a cloudy suspension after mixing of all chemicals. This was surprising, since the published procedure reported: “The suspension was treated by ultrasonic radiation to dissolve solid chemicals until a clear solution in green colour is formed.” However, in our hands the precipitate could not be dissolved even after 3 hours of sonication. A reason might be slightly different water content of solvents or starting materials. The suspension was placed into an oven, which was pre-heated to 408 K beforehand, and kept at that temperature for 3 days. The obtained green precipitate was collected by filtration, washed and activated at 443 K in dynamic vacuum for 5 hours. After activation, samples **1** and **2** were analysed by PXRD, NMR, and nitrogen physisorption.

As expected, the XRD pattern of sample 1 matches the theoretical calculated pattern of DUT-8(Ni) for the closed phase (cp) (Fig. 1a) and shows “gate opening” behaviour during the physisorption (Fig. 1b). In contrast, sample 2 shows an XRD pattern typical for the open pore phase (op) of DUT-8(Ni) (Fig. 1a) and a “Type Ia” isotherm (Fig. 1b) with a pore volume comparable to that of 1 after “gate opening”. According to the elemental analysis as well as to the ^{1}H NMR spectra after digestion of the samples, no significant differences in the composition of **1** and **2** could be found (Table S1, Fig. S6, S7, ESI).

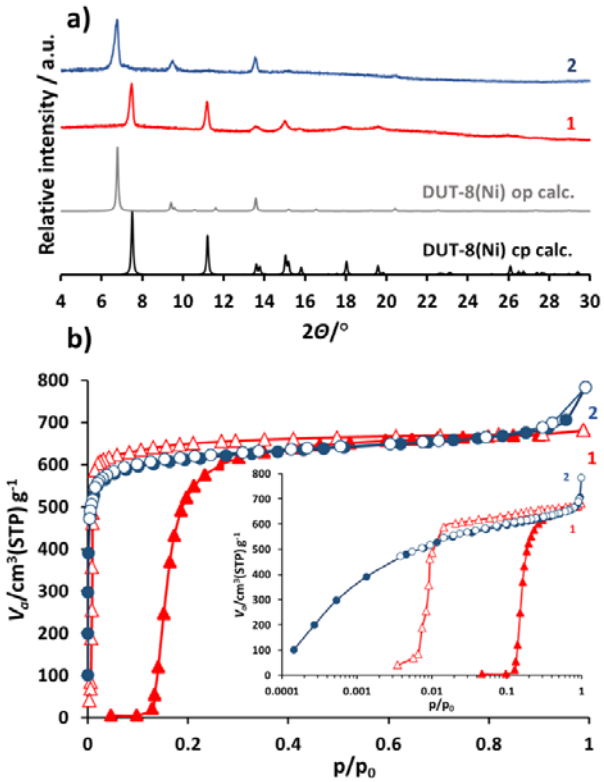

Figure 1. a) Calculated and experimental PXRD patterns of activated "flexible" (**1**) and "rigid" (**2**) DUT-8(Ni); b) Nitrogen physisorption experiments at 77 K for DUT-8(Ni) "flexible" (**1**) and "rigid" (**2**) (adsorption – filled symbols, desorption – open symbols) Inset: logarithmic plot.

In addition, we performed TG analysis in synthetic air in order to estimate the thermal stability and metal/organics ratio. Sample **1** shows slightly higher thermal stability than sample **2** and starts to decompose at 380 °C. The decomposition of **2** starts at 340 °C (Fig. S8, ESI). Decomposition of both samples proceeds in one step. In the case of sample **1** the thermal decomposition is accompanied by the formation of intermediates, which are further oxidized in the temperature range of 500 – 550 °C, causing increasing of the mass of nearly 4%. The residual mass for samples **1** and **2** is 24.12 and 23.89%, respectively, which is in a good agreement with the calculated value of 22.72%. The PXRD analyses of the residues show phase pure NiO (Fig. S9, ESI).

Thus, despite the pronounced differences in flexibility, the compositions of **1** and **2** are identical within the limits of errors of the methods. A detailed analysis of defects in lower concentration level is beyond the scope of this contribution but has been addressed recently using EPR in combination with NO adsorption.[25]

DRIFT spectra of 1 and 2 are apparently very similar (Fig. 2a). However, the spectrum of rigid compound 2 contains a few additional absorption bands at 1630, 785, and 510 cm^{-1} which are absent in the spectrum of 1. The first one could correspond to the asymmetric vibration of the carboxylic group.

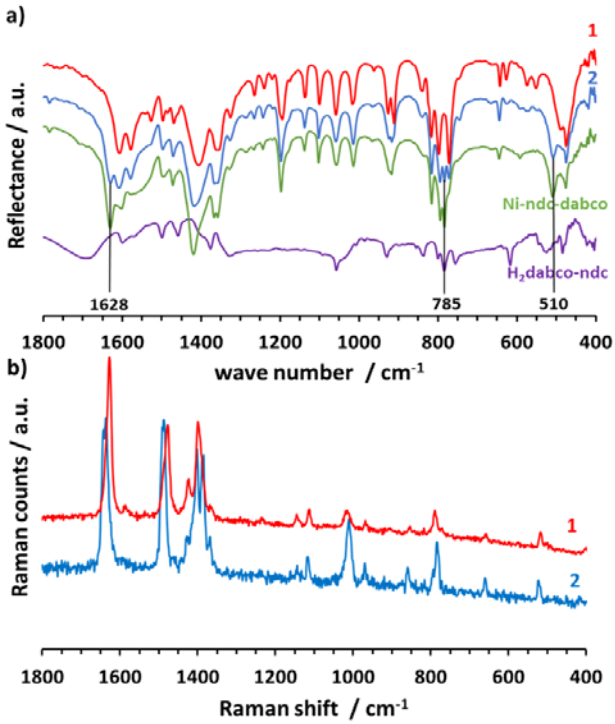

Figure 2. a) DRIFT spectra for DUT-8(Ni) "flexible" (**1**) and "rigid" (**2**), Ni-ndc-dabco, and (H_2dabco)(ndc) salt; b) Raman spectra of DUT-8(Ni) "flexible" (**1**) and "rigid" (**2**).

Therefore, the slight shift of the latter to the higher frequencies could be a sign of a different coordination mode of carboxylic groups as it could be expected for defective paddle wheels, formed because of the rapid crystallization.

The additional absorption band at 785 cm^{-1} can be assigned to the ν_sN-C3 vibration of dabco molecule.[36]

On the other hand, it is known that dabco is able to form salts with naphthoic acid where carboxylate anions are hydrogen bonded to the protonated dabco *via* $COO^-/H–N^+$ hydrogen bonds.[37] Indeed, after mixing of H_2ndc (0.294 g, 1.37 mmol) and dabco (0.336 g, 3.0 mmol) in DMF (30 mL), a white crystalline precipitate (H_2dabco)(ndc)) is formed. A DRIFT spectrum of the salt contains the absorption band at 785 cm^{-1}, exactly the same wavenumber observed for the additional band of **2** (Fig. 2).

Using the same ratio of components described for **2**, if nickel nitrate is added to the H_2ndc-dabco suspension in DMF, a green, cloudy precipitate in the following denoted as "Ni-ndc-dabco" forms. A DRIFT spectrum of this precipitate contains both additional absorption bands at 785 and 1630 cm^{-1} found in spectrum of **2**. This indicates differences in the formation pathway of **1** and **2**: For flexible **1** one may assume the direct nucleation of DUT-8(Ni), while the rigid version **2** is formed *via* an intermediate salt. The ATR-IR spectra of **1** and **2** (Fig. S14), confirm, even if less evidently, the presence of these two vibrational fingerprints of the rigid form.

The Raman spectra of **1** and **2** (Fig. 2b) are significantly different. In particular, compound **2** shows: i) in the 1700 – 1300 cm^{-1} range peaks shifted in frequency and with different relative intensity; ii) in the lower frequency range the intensity increase of the bands at 1010, 784, and 224 cm^{-1}.

Furthermore, solid state ^{13}C NMR spectra were measured on "as made" and "activated" forms of materials **1** and **2** (Fig. 3).

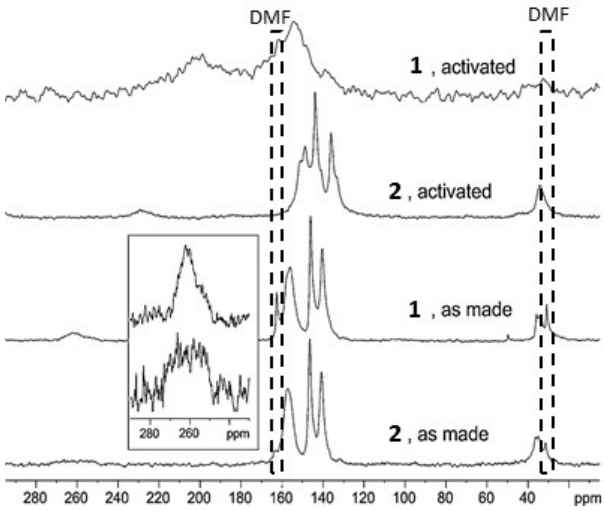

Figure 3. Solid state ^{13}C CP NMR spectra of "as made" and activated form of **1** and **2**.

The spectra of the "as made" form for **1** and **2** are almost identical and contain two signals between 30 and 40 ppm corresponding to the carbon atoms of the dabco ligand and methyl group of DMF. In the range 135 – 165 ppm, three sharp and one broad signal are observed. These signals are assigned to the five independent carbon atoms in the naphthalene core of the ndc^{2-} linker and C-H group of DMF. The broad signal of quaternary carbon of the ndc^{2-} located near the metal center is identified in the low field of NMR spectrum at 260 ppm (Inset Fig. 3).[28] Activation of the materials leads to a significant change in the ^{13}C CP NMR spectra. As it has been shown earlier,[28] activation of sample **1** leads to the broadening of all signals, belonging to the framework and disappearing of the DMF signals. The broadening of the signals could be explained either by chemical shift distribution of the carbon atoms in the **cp** phase or more restricted motions of the linkers in the **cp** compared with the **op** phase. The aforementioned chemical shift distribution could be caused by the deformation of the linker molecules as a consequence of structure closing. In the case of **2**, removal of the guest molecules from the framework has no influence on the oscillation of the carbon atoms showing no peak broadening or anisotropy. At the same time, a shift of all signals to the high field was observed and can be explained by desolvation of the framework, namely the absence of the ligand-solvent interactions.

It is interesting to note that the signal at ca. 260 ppm is considerably broader in the rigid material than in flexible DUT-8(Ni). This might be due to a larger degree of disorder (or defects) for rigid DUT-8(Ni) in agreement with EPR spectroscopic studies.[25] Thus, solid state ^{13}C NMR spectra show an essential difference between "flexible" **1** and "rigid" **2** DUT-8(Ni) in their activated form as well as absence of additional organic species.

Variation of synthesis parameters

The main difference in the synthesis procedure of "flexible" **1** and "rigid" **2** is the molar ratio of starting compounds and nature of the solvent (or more specifically solvent ratio) (Table 1). For the synthesis of the flexible version of the framework, the ratio of the nickel nitrate, H_2ndc and dabco of 1:1:0.64 is used, which is very close to the ideal composition of the resulting MOF. As the solvent a DMF/methanol mixture in volumetric ratio close to 2:1 is used. The synthesis protocol of the "rigid" **2** differs by the increased molar amount of dabco up to 2.2 equivalents in the synthesis (Table 1). Moreover, the synthesis is performed in pure DMF at slightly higher temperature.

To find out the critical parameter, which directs the formation of "flexible" or "rigid" MOF, we performed a wide variation of synthesis parameters such as molar ratio of the starting materials in the system Ni^{2+}/H_2ndc/dabco as well as solvent mixture composition, starting from original synthesis procedure for "flexible" **1** and "rigid" **2**.

In the first series, the amount of dabco was varied from 0.20 to 1.47 equivalents (samples $\mathbf{3_a}$ - $\mathbf{3_d}$), keeping all other synthetic parameters constant according to the synthetic procedure for **2.** In parallel, the syntheses were carried out under conditions used for **1** and variation of the dabco from 0.25 to 2.14 equivalents (samples $\mathbf{3'_a}$ - $\mathbf{3'_d}$).

If a lower amount of dabco is used than needed for ideal stoichiometric composition (in case of samples $\mathbf{3_a}$, $\mathbf{3_b}$ and $\mathbf{3'_a}$), the formation of a non-porous coordination polymer with composition $Ni_3(ndc)_3(DMF)_2(Me_2NH)_2$, reported earlier by Du et al.[38], was observed (Fig. 4a and 4c). It shows characteristic reflections at 2Θ = 9.22° and 9.57° in the XRD pattern, as well as an additional band at 1666 cm^{-1} in FTIR spectra, which is assigned to the coordination mode of the carboxylic group (Fig. S15, S16, ESI).

All activated samples of series **3** represent a mixture of **cp** and **op** phases. Furthermore, a decreasing intensity of the main reflection of the **cp** phase at 2Θ = 7.5° with increasing dabco content in the synthesis (samples $\mathbf{3_c}$ and $\mathbf{3_d}$) indicates the substantial role of dabco to form the targeted DUT-8(Ni) phase. Higher amounts of dabco lead also to an intensity increase of "finger print" absorption bands at 785 and 1630 cm^{-1} in $\mathbf{3_c}$ and $\mathbf{3_d}$, characteristic for the spectrum of "rigid" DUT-8(Ni) (Fig. S15, ESI).

Thus, the dabco amount has a crucial role in the synthesis triggering the formation of small amounts of "flexible" DUT-8 (**1**) if utilised in lower concentrations. However, pure "flexible" **1** could not be obtained and very low dabco amounts utilised in the synthesis, caused a

dense phase formation containing no dabco. In contrast, samples **b** - **c** of series **3'**, synthesized in DMF:MeOH mixture, are pure **cp** phase according to the XRD (Fig. 3) and DRIFT (Fig. S16, ESI) analyses. Sample **3'$_d$** shows only a minor impurity of **op** phase. Thus methanol has an essential influence on the phase formation.

Therefore, in the next step the role of solvent composition was further explored in series **4**. Keeping the $Ni^{2+}/H_2ndc/dabco$ ratio constant (1.1:1:2.2), the MeOH content in DMF was varied from 1.6% to 36% (MeOH content in the typical synthesis of flexible **1** is 30%).

PXRD patterns of the samples **4$_a$** and **4$_b$**, synthesized using only minor amounts of methanol, show exclusively **op** phase of the MOF. Only if the methanol concentration is higher than 20%, a **cp**/**op** phase mixture is formed. It is also reflected in the decreasing intensity of IR absorption bands at 1630 and 785 cm^{-1} (Fig. S17, ESI).

Finally, in series **5** and **5'** we could show, that the amount of Ni^{2+} does not influence the formation of expected phases, and independent of nickel amount utilized (within the investigated range) the resulting crystalline phase is mostly solvent directed (Fig. S1, ESI). Similar to results obtained *via* PXRD and SEM techniques, the variation of the nickel amount in the synthesis causes no changes in the DRIFT spectra (Fig. S18, ESI).

Nitrogen and argon physisorption

One of the main differences between the "flexible" and "rigid" DUT-8(Ni) materials is the response during nitrogen adsorption at 77 K and thus physisorption experiments are an ideal technique to distinguish the switchability behaviour of samples prepared under various conditions as the isotherms differ significantly in slope but show a comparable total pore volume (Fig. 1b). For investigation of the pore size distribution in MOFs, argon physisorption at 87 K was used as it is recommended (Fig. S3, ESI).[39] The experimental micropore volume (V_p) of 0.97 cm^3g^{-1} and BET surface area (S_{BET}) of 2635 m^2g^{-1} derived from Ar adsorption isotherm are in perfect agreement with values calculated using Poreblazer from the crystal structure of DUT-8(Ni) (V_p = 0.99 cm^3g^{-1}, S = 2528 m^2g^{-1}). For calculating the pore size distribution NLDFT was applied (zeolite/silica adsorption branch kernel based on a cylindrical pore model). The obtained pore size distribution plot has a maximum at 8.7 Å. This value is by 1.1 Å smaller than the value calculated geometrically using Poreblazer software for DUT-8(Ni) op structure (Fig. S4 and S5 ESI).[40] The largest included sphere, calculated for the structure, has a diameter of 10.0 Å. Given the limitations of the NLDFT kernels, the pore size calculated from the adsorption isotherm and crystal structure are not in excellent but reasonable agreement. We assume that the desorption branch of the isotherm represents the thermodynamic equilibrium of the switching process as for closing no diffusional activation barrier has to be overcome (Fig. 1b inset). In the case of "flexible" material **1**, this "gate closing" pressure is observed at p/p_0 = 0.01, and the structural transformation from **op** to **cp** takes place accompanied by the sharp drop in nitrogen uptake from 588 cm^3g^{-1} at p/p_0 = 0.015 to 40 cm^3g^{-1} at p/p_0 = 0.003.

In contrast, the desorption branch of **2** matches the adsorption branch without any hysteresis, indicating no structural changes in the sample during physisorption.

Nitrogen adsorption isotherms for samples from the series **3** and **3'** reflect the findings from the XRPD analysis. All samples of series **3** show isotherms characteristic for flexible MOFs, but are different from typical isotherms usually obtained for "gate pressure" MOFs. In fact, nitrogen adsorption isotherms of **3$_a$** - **3$_d$** are a superposition of the isotherms characteristic for **1** and **2.** Therefore the pore volume, calculated from nitrogen uptake plateau before "gate opening" can be attributed to the amount of the "rigid" phase in the sample. The ratio between this value and total pore volume represents the ratio between the amounts of "rigid" and flexible phases and is 35:65 for samples **3$_a$** and **3$_b$** and 56:44 for samples **3$_c$** and **3$_d$**.

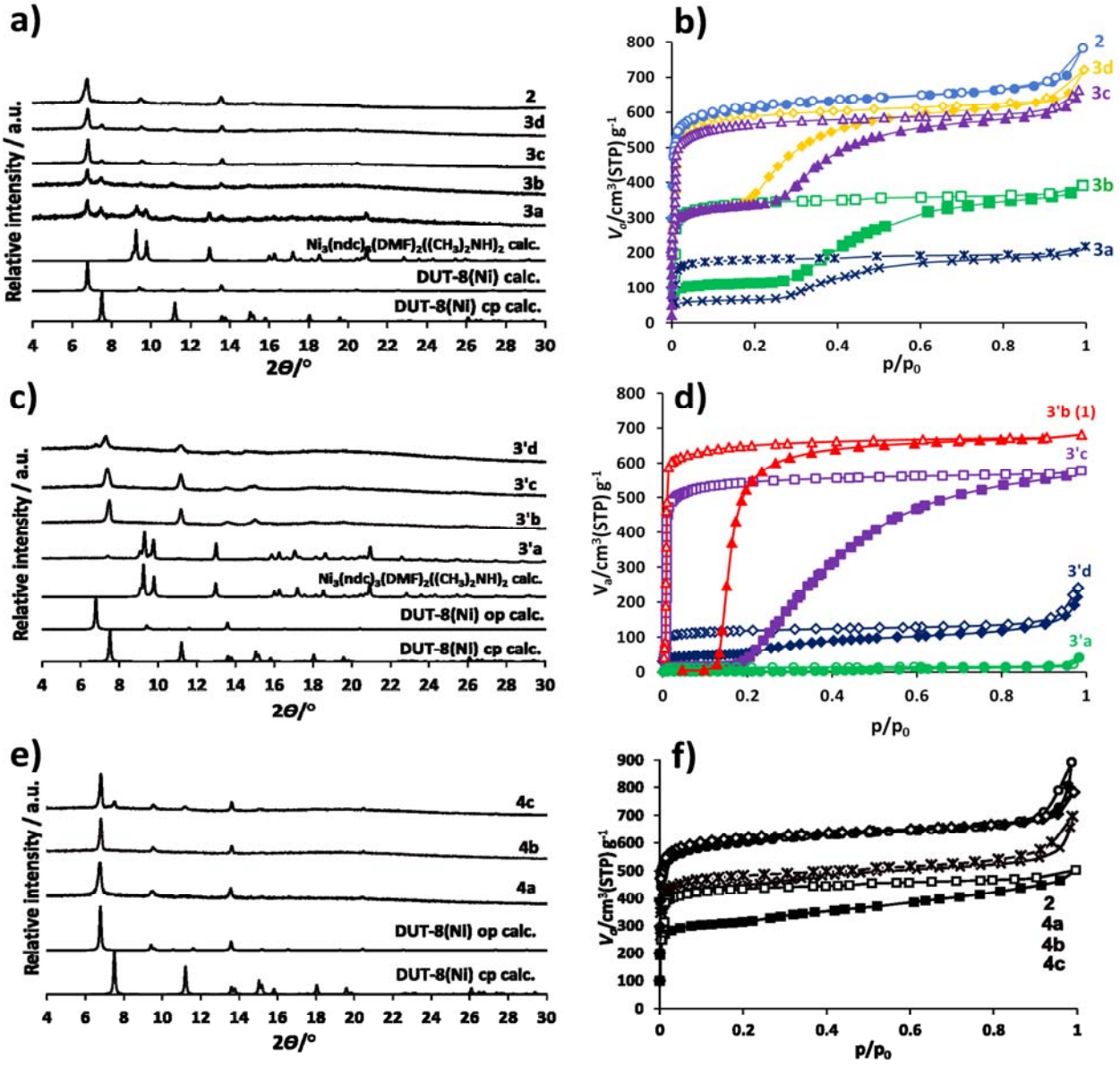

As expected, sample $\mathbf{3'_a}$ of the composition $Ni_3(ndc)_3(DMF)_2(Me_2NH)_2$ has no porosity in the crystal structure and therefore shows nearly no nitrogen uptake (Fig. 4d). The samples $\mathbf{3'_b}$ and $\mathbf{3'_c}$ show "gate opening" behaviour, but slightly different uptake in saturation.

Further increasing of dabco amount in the synthesis of $\mathbf{3'_d}$ leads to a significant drop in the total pore volume and changes the isotherm slope in the gate region (Fig. 4d).

Interestingly, the "gate opening" pressure is influenced by the synthetic conditions and is shifted to higher relative pressure from p/p_0 = 0.13 for **1** to p/p_0 = 0.16 in the $\mathbf{3_d}$ and to p/p_0 = 0.28 for the samples $\mathbf{3_a}$, $\mathbf{3_b}$, $\mathbf{3_c}$ and $\mathbf{3'_c}$. An interesting observation is that significant differences in the "gate opening" pressure are observed (for example for $\mathbf{3'_b}$ and $\mathbf{3'_c}$) while the "gate closing" pressure is essentially the same (Fig. S2b, ESI). These differences are representative for cooperative switching in single crystallites (or agglomerates) within the particle ensemble (see also particle size analysis) and indicate their strong influence of the activation barrier for opening (kinetics) while the closing energetics (equilibrium) are not affected (Fig. S2a, S2b, ESI). A steep slope at "gate opening" is indicative for a particle ensemble with relatively uniform activation barrier, while a broadening indicates a broader distribution of activation barriers. Similar phenomena were observed recently by repeated adsorption/desorption of *n*-butane on flexible DUT-8(Ni) and was attributed to the dislocations and lattice strain within the crystallites.[27]

According to XRD analysis, samples $\mathbf{4_a}$ and $\mathbf{4_b}$ (prepared using the reported synthetic procedure for "rigid" DUT-8, but using various DMF:MeOH ratios) represent the **op** phase. In sample $\mathbf{4_c}$ additionally a minor fraction of **cp** phase is detected. However, the nitrogen adsorption experiments reveal an unexpected adsorption behaviour: An increasing methanol content in the synthesis leads to a gradual

decrease of the porosity and total pore volume. Sample **4$_c$** shows also a broad hysteresis in the whole pressure range (Fig. 4f), indicating the presence of the "flexible" phase.
In contrast, the variation of the amount of Ni^{2+} in the synthesis has only minor influence on both products, and the nitrogen adsorption isotherm, measured on the sample **5´$_a$**, synthesized using the procedure for "flexible" DUT-8(Ni) but only 50% of the Ni^{2+} in the synthesis, reaches the same total pore volume in saturation, but shows a significantly broadened "gate opening" (Fig. S1b, ESI). The variation of the nickel amount in the procedure for "rigid" DUT-8(Ni) influences only the total pore volume of resulting materials **5$_a$ - 5$_b$** (Fig. S1d, ESI), but very little the shape of the isotherm.

Particle size

Recently the influence of crystallite size on adsorption induced phase transitions has been recognized.[9, 33, 41] Kitagawa and co-workers reported that downsizing of twofold interpenetrated frameworks of Cu_2(dicarboxylate)$_2$(amine) regulates the structural flexibility and may induce shape-memory effects in coordination frameworks.[33] The downsizing of the ZIF-8 crystallites was shown to suppress ligand flip during adsorption.[34] Consequently, an important aspect was to analyze the particle size of the products obtained in the syntheses under varying conditions.
SEM images of DUT-8(Ni) "flexible" **1** show relatively large crystallites with a size ranging from 20 to 100 µm, which is fully consistent with our previous study (Fig. 5).[27] In contrast, images obtained for DUT-8(Ni) "rigid" **2**, show a particle size magnitude close to the resolution limit of the SEM instrument. In general, the poor electrical conductivity of MOFs is disadvantageous for high-resolution SEM studies. Nevertheless, a rough estimation results in an average particle size of 200 - 500 nm (Fig. 5).
In the samples **3$_a$** and **3$_b$**, where an additional non-porous phase of $Ni_3(ndc)_3(DMF)_2(Me_2NH)_2$ is observed in PXRD, SEM images contain beside the typical bricks of DUT-8(Ni) also some spherical particles, which may be attributed to $Ni_3(ndc)_3(DMF)_2(Me_2NH)_2$ (Fig. S10, ESI). Images of **3$_a$** – **3$_d$** show a broad particle size distribution for DUT-8(Ni) (Fig. S10, ESI). Particles larger than 50 µm as well as very small particles (< 1 µm) can be observed in the images. This observation is consistent with the results from PXRDs and isotherms showing the presence of both **cp** and **op** phases and 2 steps in the nitrogen adsorption isotherms, if one assumes that only crystals exceeding a critical size may lead to switchability. The broadened "gate pressure" in the isotherms of **3$_a$ - 3$_d$**, in this interpretation, can be considered as originating from a broad particle size distribution in these samples. As for many cooperative phenomena, it is reasonable to expect that the activation energy for "gate opening" is related to the crystallite size. In this interpretation, depending on the crystallite size, the crystallites open from **cp** to **op** at different pressure while the closing pressure is not affected. However, this interpretation is oversimplified, since the first guest removal (activation) process causes larger crystals to transform into an intertwined domain structure in which the domain size and the grain boundary energy determines the activation energy. As the solvothermal synthesis results in the formation of the **op** phase, the desolvation procedure is decisive in affecting the microstructure. Due to the huge crystal contraction during solvent removal, larger crystals disintegrate into a complex microstructure with grain boundaries of unknown size creating an interfacial domain area A_{id} as explained above. A uniform microstructure with grains of similar size will afford a steep gate opening characteristic, as the activation energy for switching the microdomains is identical. We expect **op** crystals differing in size to afford differently sized microdomain structures upon desolvation into the cp phase, and hence altered activation energies corresponding to altered gate opening pressures. We hypothesize grain boundaries to act as the nucleation sites for the gating transition as they may act as diffusional entries for the gas. Thus, for smaller crystals fewer number of grain boundaries and defect statistics could in principle even shift the gate opening pressure so far, that the crystals remain closed in the whole pressure range. This hypothesis could explain the significantly reduced maximum uptake in some samples with intermediate particle size. If a crystal approaches a certain lower boundary, we can expect a single domain switching mechanism without fracture into mirodomains similar to other ferroic size phenomena. Below this critical size only A_o will determine the gate opening pressure. However, crystals varying in size may also differ in point defect concentration and small variations in defect concentration can also change the activation barrier.

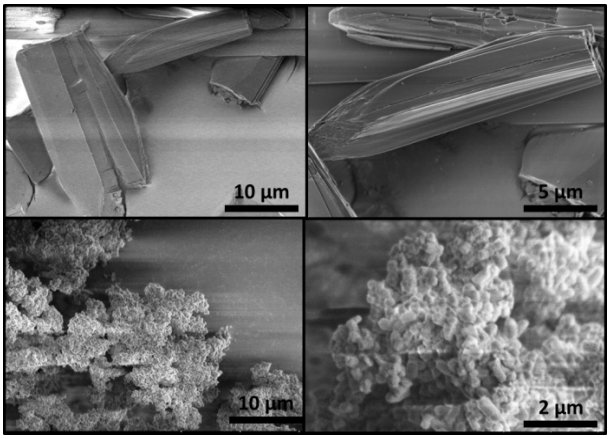

Figure 5. SEM images: flexible DUT-8(Ni) (**1**) (top) and rigid DUT-8(Ni) (**2**) (bottom).

In our observations, below a critical size, which for DUT-8(Ni) we estimate based on this study to be approximately 500 nm, the material does not transform into the closed form by the guest removal (activation), and an isotherm typical for rigid microporous materials is observed. The underlying principle for this observation must rely on a thermodynamic stabilization of the **op** *vs.* **cp** phase as this phenomenon is observed in vacuum without any gases. A possible explanation relies on the EPR data, and the recently identified high defect concentrations[25] could arise from rapid nucleation and growth. Especially missing ndc ligands are expected to reduce the dispersive energetic stabilization of DUT-8(Ni) **cp**. Another potential explanation could be differences in surface energy related to A_o. However, as A_O is larger for the **op** phase ($A_o = A_o$(**op**) - A_o(**cp**) > 0), this explanation would imply the specific surface energy difference as = (**op**) - (**cp**) < 0 which is difficult to justify.

Zhang et al. proposed an explanation for the thermodynamically controlled crystal-size-dependent structural transitions in MOFs in the presence of gases. The calculations showed, that the suppressed adsorption uptake at the surface of nanoparticles compared to that at the bulk-like region results in a reduced thermodynamic driving force for the transition in the nanoparticle over the entire range of bulk fluid pressures.[34]

Form an experimental point of view, the overall trend is consistent for all synthesis parameters. In the sample series **3'**, the changes of the dabco amount also strongly affect the crystallite size. The SEM images sample **3'$_a$** show block-like overgrown crystallites, which according to the XRD should belong to the $Ni_3(ndc)_3(DMF)_2(Me_2NH)_2$ phase (Fig. S11, ESI). Obviously, the use of methanol in the synthesis creates the best conditions for growing larger crystals. Increased amount of dabco in the samples **3'$_c$** and **3'$_d$** leads to a broadening of the particle size distribution as it can be directly observed in the images showing crystallites ranging from several hundred nanometer to hundred micrometre size. Again, these effects are indirectly reflected in the PXRD showing mixtures of two phases and nitrogen adsorption isotherms with broadened gating transitions. The gradual increase of the methanol amount in the mixture in the sample series **4** shows a very similar effect. The sample **4$_a$** synthesized with lowest methanol content consists of the crystallites with maximal size of 500 nm and therefore shows pure "Type Ia" isotherm and the **op** phase in the PXRD. With increasing methanol amount in the synthesis, the particle size distribution is broadened. In sample **4$_c$** the particle size is ranging from 500 nm to 10 µm (Fig. S12, ESI) also reflecting well the nitrogen adsorption and PXRD experiments (Fig. 4e-f). As expected from the isotherms and XRD measurements, the variation of the nickel amount in the synthesis does not influence the particle size in samples **5'$_a$** and **5'$_b$** (Fig. S13, ESI).

Temperature dependent X-ray diffraction study

Kitagawa and co-worker reported, that for interpenetrated pillared-layer compound $Cu_2(bdc)_2(bpy)$ (bdc = 1,4-benzenedicarboxylate, bpy = 4,4'-bipyridine) the pore shape could be switched from the open to the closed form by heating. Thus, temperature dependent X-ray diffraction experiments were conducted on **2** (Fig. 6, Fig. S19) to investigate the behavior of DUT-8 during heating. However, the rigid DUT-8 remains in the open form until decomposition and therefore is not temperature responsive.

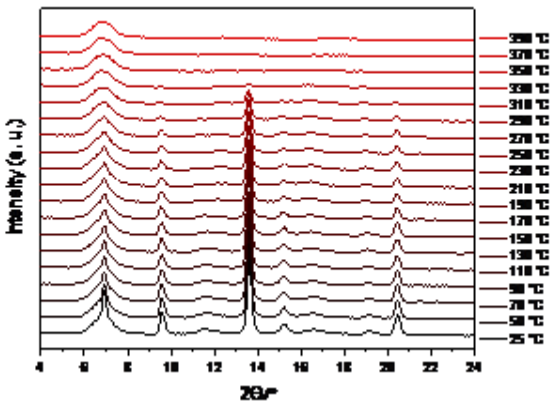

Figure 6. Temperature dependent X-ray diffraction patterns of **2** heated in vacuum.

Conclusions

Significant differences in the synthesis pathway were found to be responsible for the formation of "rigid" and "flexible" DUT-8(Ni) under different synthesis conditions. The high supersaturation in the synthesis of "rigid" DUT-8(Ni) causes the formation of intermediate phases and rapid nucleation, leading to small and defective crystallites showing typical type I physisorption isotherms. In contrast, the higher solubility provided in the crystallization of "flexible" DUT-8(Ni) and slow crystallization causes the formation of large crystals that can undergo a transformation into a closed phase upon desolvation. Samples with crystallites smaller than 500 nm do not show the op → cp phase transformation and therefore stay in the open form after the guest molecules removal, whereas particles larger than 1 µm can be reversibly transformed into the cp phase.

For “flexible” DUT-8(Ni), varied synthesis parameters influencing the crystal size can be used to tune the “gate opening” pressure reflecting the activation barrier of the phase transition, while the “gate closing” pressure remains constant.
The reason for a strong effect of synthesis parameters lies in the differences of the crystallization mechanism: An excess amount of the dabco in the synthesis of the “rigid” DUT-8(Ni) is partially consumed by deprotonation of the H_2ndc ligand resulting in the absence of metal source and the precipitation of a (H_2dabco)(ndc) salt. In the presence of Ni^{2+} cations, rapid nucleation of the defective DUT-8(Ni) structure proceeds in the form of a cloudy microcrystalline precipitate. High concentration of defects in this phase was recently confirmed by EPR in the presence of NO. Additional bands in the IR-spectrum support these findings. Thus particle size and defects are both decisive factors influencing flexibility. In contrast, the use of stoichiometric ratio of the initial reagents in the crystallization of “flexible” DUT-8(Ni) in DMF/methanol mixture inhibits complete deprotonation of H_2ndc and therefore slows down the nucleation and crystallization of the target compound. It causes the formation of large crystals (20 to 100 µm). These large crystals undergo a transformation into a closed phase upon desolvation.
An important implication of our findings is that switchable MOFs, especially those showing pronounced volume changes, should always be considered as materials with “history dependent adsorption profiles”, because each transition undergone may cause changes in domain size and defect formation which in turn affects the adsorption behaviour. We believe our findings to be an important step towards a fundamental understanding of adsorption induced switching transitions of porous solids.

Acknowledgements

Financial support by the “excellence initiative by German federal and state government” (measure “support the best”) and DFG (FOR 2433) is gratefully acknowledged. V.B. acknowledges German Federal Ministry of Education and Research (BMBF Project No 05K16OD1) for the financial support. Authors are very grateful to Prof. S. Bordiga for the valuable discussions of the IR and Raman spectra.

References

- 1. S. Horike, S. Shimomura and S. Kitagawa, *Nat. Chem.*, 2009, **1**, 695-704.
- 2. G. Ferey and C. Serre, *Chem. Soc. Rev.*, 2009, **38**, 1380-1399.
- 3. Z. Chang, D.-H. Yang, J. Xu, T.-L. Hu and X.-H. Bu, *Adv. Mater.*, 2015, **27**, 5432-5441.
- 4. F.-X. Coudert, *Chem. Mater.*, 2015, **27**, 1905-1916.
- 5. A. Schneemann, V. Bon, I. Schwedler, I. Senkovska, S. Kaskel and R. A. Fischer, *Chem. Soc. Rev.*, 2014, **43**, 6062-6096.
- 6. A. Kondo, H. Noguchi, S. Ohnishi, H. Kajiro, A. Tohdoh, Y. Hattori, W.-C. Xu, H. Tanaka, H. Kanoh and K. Kaneko, *Nano Lett.*, 2006, **6**, 2581-2584.
- 7. T. R. C. Van Assche, G. V. Baron and J. F. M. Denayer, *Dalton Trans.*, 2016, **45**, 4416-4430.
- 8. T. Song, J. Yu, Y. Cui, Y. Yang and G. Qian, *Dalton Trans.*, 2016, **45**, 4218-4223.
- 9. O. M. Linder-Patton, W. M. Bloch, C. J. Coghlan, K. Sumida, S. Kitagawa, S. Furukawa, C. J. Doonan and C. J. Sumby, *CrystEngComm*, 2016, **18**, 4172-4179.
- 10. M. L. Foo, R. Matsuda, Y. Hijikata, R. Krishna, H. Sato, S. Horike, A. Hori, J. Duan, Y. Sato, Y. Kubota, M. Takata and S. Kitagawa, *J. Am. Chem. Soc.*, 2016, **138**, 3022-3030.
- 11. J. A. Mason, J. Oktawiec, M. K. Taylor, M. R. Hudson, J. Rodriguez, J. E. Bachman, M. I. Gonzalez, A. Cervellino, A. Guagliardi, C. M. Brown, P. L. Llewellyn, N. Masciocchi and J. R. Long, *Nature*, 2015, **527**, 357-361.
- 12. H. Sato, W. Kosaka, R. Matsuda, A. Hori, Y. Hijikata, R. V. Belosludov, S. Sakaki, M. Takata and S. Kitagawa, *Science*, 2014, **343**, 167-170.
- 13. R. Matsuda, *Nature*, 2014, **509**, 434-435.
- 14. P. Serra-Crespo, M. A. van der Veen, E. Gobechiya, K. Houthoofd, Y. Filinchuk, C. E. A. Kirschhock, J. A. Martens, B. F. Sels, D. E. De Vos, F. Kapteijn and J. Gascon, *J. Am. Chem. Soc.*, 2012, **134**, 8314-8317.
- 15. N. Yanai, K. Kitayama, Y. Hijikata, H. Sato, R. Matsuda, Y. Kubota, M. Takata, M. Mizuno, T. Uemura and S. Kitagawa, *Nat. Mater.*, 2011, **10**, 787-793.
- 16. K. Nakagawa, D. Tanaka, S. Horike, S. Shimomura, M. Higuchi and S. Kitagawa, *Chem. Commun.*, 2010, **46**, 4258-4260.
- 17. F.-X. Coudert, A. Boutin, A. H. Fuchs and A. V. Neimark, *J. Phys. Chem. Lett.*, 2013, **4**, 3198-3205.
- 18. H. Tanaka, S. Ohsaki, S. Hiraide, D. Yamamoto, S. Watanabe and M. T. Miyahara, *J. Phys. Chem. C*, 2014, **118**, 8445-8454.
- 19. D. Li and K. Kaneko, *Chem. Phys. Lett.*, 2001, **335**, 50-56.
- 20. V. Bon, I. Senkovska, D. Wallacher, A. Heerwig, N. Klein, I. Zizak, R. Feyerherm, E. Dudzik and S. Kaskel, *Microporous Mesoporous Mater.*, 2014, **188**, 190-195.
- 21. Y. Cheng, H. Kajiro, H. Noguchi, A. Kondo, T. Ohba, Y. Hattori, K. Kaneko and H. Kanoh, *Langmuir*, 2011, **27**, 6905-6909.
- 22. H. Kanoh, A. Kondo, H. Noguchi, H. Kajiro, A. Tohdoh, Y. Hattori, W.-C. Xu, M. Inoue, T. Sugiura, K. Morita, H. Tanaka, T. Ohba and K. Kaneko, *J. Colloid Interface Sci.*, 2009, **334**, 1-7.
- 23. S. Hiraide, H. Tanaka and M. T. Miyahara, *Dalton Trans.*, 2016, **45**, 4193-4202.

- 24. D. N. Dybtsev, H. Chun and K. Kim, *Angew. Chem. Int. Ed.*, 2004, **43**, 5033-5036.
- 25. M. Mendt, F. Gutt, N. Kavoosi, V. Bon, I. Senkovska, S. Kaskel and A. Pöppl, *J. Phys. Chem. C*, 2016, **120**, 14246-14259.
- 26. V. Bon, N. Klein, I. Senkovska, A. Heerwig, J. Getzschmann, D. Wallacher, I. Zizak, M. Brzhezinskaya, U. Mueller and S. Kaskel, *Phys. Chem. Chem. Phys.*, 2015, **17**, 17471-17479.
- 27. V. Bon, N. Kavoosi, I. Senkovska and S. Kaskel, *ACS Appl. Mater. Interfaces*, 2015, **7**, 22292-22300.
- 28. N. Klein, H. C. Hoffmann, A. Cadiau, J. Getzschmann, M. R. Lohe, S. Paasch, T. Heydenreich, K. Adil, I. Senkovska, E. Brunner and S. Kaskel, *J. Mater. Chem.*, 2012, **22**, 10303-10312.
- 29. N. Klein, C. Herzog, M. Sabo, I. Senkovska, J. Getzschmann, S. Paasch, M. R. Lohe, E. Brunner and S. Kaskel, *Phys. Chem. Chem. Phys.*, 2010, **12**, 11778-11784.
- 30. K. Trepte, S. Schwalbe and G. Seifert, *Phys. Chem. Chem. Phys.*, 2016, **18**, 1348.
- 31. H. C. Hoffmann, B. Assfour, F. Epperlein, N. Klein, S. Paasch, I. Senkovska, S. Kaskel, G. Seifert and E. Brunner, *J. Am. Chem. Soc.*, 2011, **133**, 8681-8690.
- 32. J. Y. Lee, L. Pan, X. Huang, T. J. Emge and J. Li, *Adv. Funct. Mater.*, 2011, **21**, 993-998.
- 33. Y. Sakata, S. Furukawa, M. Kondo, K. Hirai, N. Horike, Y. Takashima, H. Uehara, N. Louvain, M. Meilikhov, T. Tsuruoka, S. Isoda, W. Kosaka, O. Sakata and S. Kitagawa, *Science*, 2013, **339**, 193-196.
- 34. C. Zhang, J. A. Gee, D. S. Sholl and R. P. Lively, *J. Phys. Chem. C*, 2014, **118**, 20727-20733.
- 35. S. Watanabe, S. Ohsaki, T. Hanafusa, K. Takada, H. Tanaka, K. Mae and M. T. Miyahara, *Chem. Eng. J.*, 2017, **313**, 724-733.
- 36. D. A. Guzonas and D. E. Irish, *Can. J. Chem.*, 1988, **66**, 1249-1257.
- 37. A. Jacobs, L. R. Nassimbeni, G. Ramon and B. K. Sebogisi, *CrystEngComm*, 2010, **12**, 3065-3070.
- 38. Y. Du, A. L. Thompson, N. Russell and D. O'Hare, *Dalton Trans.*, 2010, **39**, 3384-3395.
- 39. M. Thommes, K. Kaneko, A. V. Neimark, J. P. Olivier, F. Rodriguez-Reinoso, J. Rouquerol and K. S. W. Sing, *Pure Appl. Chem.*, 2015, **87**, 1051-1069.
- 40. L. Sarkisov and A. Harrison, *Mol. Simul.*, 2011, **37**, 1248-1257.
- 41. S. Tanaka, K. Fujita, Y. Miyake, M. Miyamoto, Y. Hasegawa, T. Makino, S. Van der Perre, J. C. Saint Remi, T. Van Assche, G. V. Baron and J. F. M. Denayer, *J. Phys. Chem. C*, 2015, **119**, 28430-28439.